Extraocular muscle deformation assessed by motion-encoded MRI during eye movement in healthy subjects

Marco Piccirelli — Institute for Biomedical Engineering, University and ETH Zurich, Zurich, Switzerland, & Department of Ophthalmology, University Hospital of Zurich, Zurich, Switzerland

Roger Luechinger — Institute for Biomedical Engineering, University and ETH Zurich, Zurich, Switzerland

Andrea K. Rutz — Institute for Biomedical Engineering, University and ETH Zurich, Zurich, Switzerland

Peter Boesiger — Institute for Biomedical Engineering, University and ETH Zurich, Zurich, Switzerland

Oliver Bergamin — Department of Ophthalmology, University Hospital of Zurich, Zurich, Switzerland

Conventional magnetic resonance imaging (MRI) is useful for assessing morphological changes but not for assessing deformations inside homogeneous structures (M. D. Abràmoff, A. P. Van Gils, G. H. Jansen, & M. P. Mourits, 2000). Since no intrinsic contrast can be imaged for distinguishing heterogeneous patterns of muscle contraction, morphological changes along the length of the extraocular muscles (EOMs) are not macroscopically detectable. However, an imaging method that is able to directly encode motion could give evidence about the dynamics of the inhomogeneous deformation of the EOMs. Thus, we developed a method for acquiring motion-encoded MRI images of the EOMs during eye movements. Seven healthy subjects gazed at a horizontal sinusoidally oscillating target. A small surface coil was placed in front of the right orbit. The contracting and relaxing horizontal rectus muscles and the noncontracting optic nerve were reliably tracked. The differential contractility of the EOMs could be distinguished from the third time frame on (=140 ms from the beginning of the right to left eye movement lasting 1 s). The muscle belly of the contracting medial rectus muscle could be distinguished from the posterior and the anterior segment from the sixth time frame on (=350 ms). In conclusion, motion-encoded MRI resolved the heterogeneous contraction of moving EOM segments in healthy subjects without using physical markers.

Keywords: motion-encoded MRI, tagging, physiology of extraocular muscle movement

Citation: Piccirelli, M., Luechinger, R., Rutz, A. K., Boesiger, P., & Bergamin, O. (2007). Extraocular muscle deformation assessed by motion-encoded MRI during eye movement in healthy subjects. *Journal of Vision, 7*(14):5, 1–10, http://journalofvision.org/7/14/5/, doi:10.1167/7.14.5.

Introduction

The pattern of movement within the extraocular muscles (EOMs) and the surrounding orbital connective tissue is not yet understood (Miller, Rossi, Wiesmair, Alexander, & Gallo, 2006). Knowledge about the physiology of the contractility pattern of the EOMs during eye movement is essential to understanding the pathology progression in diseases that affect the EOMs. So far, visualization of the EOM path by magnetic resonance imaging (MRI) has been restricted to multi-positional imaging.

However, the MRI signal has been known to be sensitive to motion since the fifties (Suryan, 1951). First applied to measure blood flow in healthy subjects (Morse & Singer, 1970), the tagging of tissue magnetization was introduced in 1988 to depict the heart deformation within an image plane (Zerhouni, Parish, Rogers, Yang, & Shapiro, 1988). Further improved by Axel and Dougherty (1989) and Fischer, Mckinnon, Maier, and Boesiger (1993), this method was later adapted to other tissues, e.g., the brain (Soellinger, Ryf, Boesiger, & Kozerke, 2007).

Motion-encoded MRI is able to capture the motion of tissues relative to a fixed spatial referential system. The motion of tissue points can even be visually tracked

doi: 10.1167/7.14.5 Received April 20, 2007; published November 21, 2007 ISSN 1534-7362

directly from the MR images without postprocessing, as will be shown later in the first two figures. This method will permit detailed studies of normal EOMs in vivo and depict the deformation of soft orbital tissues during smooth movements of the eye. The objective of this study was to take advantage of motion-encoded MRI to measure the heterogeneous deformation *along* the lateral and medial rectus muscles and the optic nerve in healthy subjects.

This study contains three parts. First, we present images that can be obtained with motion-encoded MRI and analyze their dissimilarities with conventional MRI (Figure 1). For objective measurement of the relative motion of tissue points, an automatic tracking method is used (Figure 2). The second part of this study tests the reliability of the tracking method. Using a supramillimetric resolution in this study, we tracked several neighboring tissue points that are expected to have a similar motion and investigated the variation of the results (Figures 3 and 4). The third part presents the physiological data that were obtained (Figures 5 and 6).

Methods

Subjects and setup

The study was conducted according to the tenets of the Declaration of Helsinki and approved by the local ethics committee. Nine subjects were recruited for the imaging part of the study, and informed consent was obtained from the subjects after explanation of the nature and possible consequences of the study. The visual acuity of all subjects was sufficient to track the visual stimulus described below. To compare the deformation of the EOMs with the optic nerve (ON), we required the complete muscles and ON to be visible within one image plane of 4 mm thickness. Therefore, two subjects with a strongly curved ON were excluded because their ON could not be completely visualized in the same transversal image plane as the horizontal EOMs. Seven healthy volunteers (two women and five men; mean age: 36 years; range: 27 to 62 years of age) were included for further analysis.

MR images of the right orbit were acquired using a small receive-only surface coil (47 mm diameter) on a 1.5 T system (Achieva 1.5 T; Philips Medical Systems, Best, The Netherlands). Small surface coils have a greater signal to noise ratio (SNR) that declines faster with depth than larger coils. Preliminary experiments showed, however, that the microscopy coil used still had a better SNR for the orbital apex than the next bigger surface coil in our possession. The microscopy coil was placed like a monocle, so that it was possible to see the target through it. The head of the subject was immobilized with foam pads. A typical functional MRI setup (computer projector, screen, and the software "Presentation"—Neurobehavioral Systems Inc., Albany CA, USA) was used for the presentation of the visual stimulus. A mirror allowed the subjects to gaze out of the bore to the projection screen. The horizontal gaze range was 40 deg. The room light was turned off to maximize the contrast of the stimulus.

Stimulus paradigms

A horizontal sinusoidally oscillating white square (target size = 0.4 deg, luminance = 5.1 ± 1 cd/mm^2 on a background of 0.05 ± 0.02 cd/mm^2) with an amplitude of ±20 deg and a period of 2 s (corresponding to a maximal target velocity of 64 deg/s) was presented on a black background to induce smooth pursuit eye movements. It is known that humans can pursue targets moving at 60 deg/s rather well (Meyer, Lasker, & Robinson, 1985). Preliminary experiments using scleral search coils confirmed that a maximal target speed of 64 deg/s induced only few catch-up saccades, see also Figure 3 in (Yee, Goldberg, Jones, Baloh, & Honrubia, 1983). These preliminary experiments were done on a subgroup of the same subjects outside the scanner bore. The results at this velocity confirmed that indeed only a negligible number of catch-up saccades were present. During preparation, all subjects confirmed the target was visible at all times. The sinusoidal oscillation of the target was repeated for approximately 4.5 min. Images were acquired on all subjects from right to left horizontal gaze. A slight up-gaze position, dependent on the subjects' anatomy, was necessary for imaging the ON in the same plane as the horizontal rectus muscles.

MRI sequence

Transversal MR images were acquired with a fast gradient echo sequence. The right-to-left horizontal eye movement of 40 deg was split into fifteen time frames of 70 ms (1050 ms acquisition period). The remaining 950 ms of the 2 s periodic eye movement served for signal recovery. The relatively short time frame duration of 70 ms was chosen so that the deformation of the orbital tissues between two time frames was small enough to allow tracking. The following scan parameters were selected: field of view: 140 × 140 mm^2 (big enough to avoid fold over artifacts), scan resolution: 1.2 × 1.2 × 4.0 mm^3 (limited by scan duration and signal to noise ratio), number of signal averages: 8 (to increase the signal to noise ratio), reconstruction matrix 256 × 256. The use of an echo planar imaging (EPI) factor of 5 shortened the acquisition time to 4.5 min.

The MRI sequence CSPAMM (Complementary SPAtial Modulation of Magnetization) (Fischer et al., 1993) encodes the motion of each tissue point. Before the images

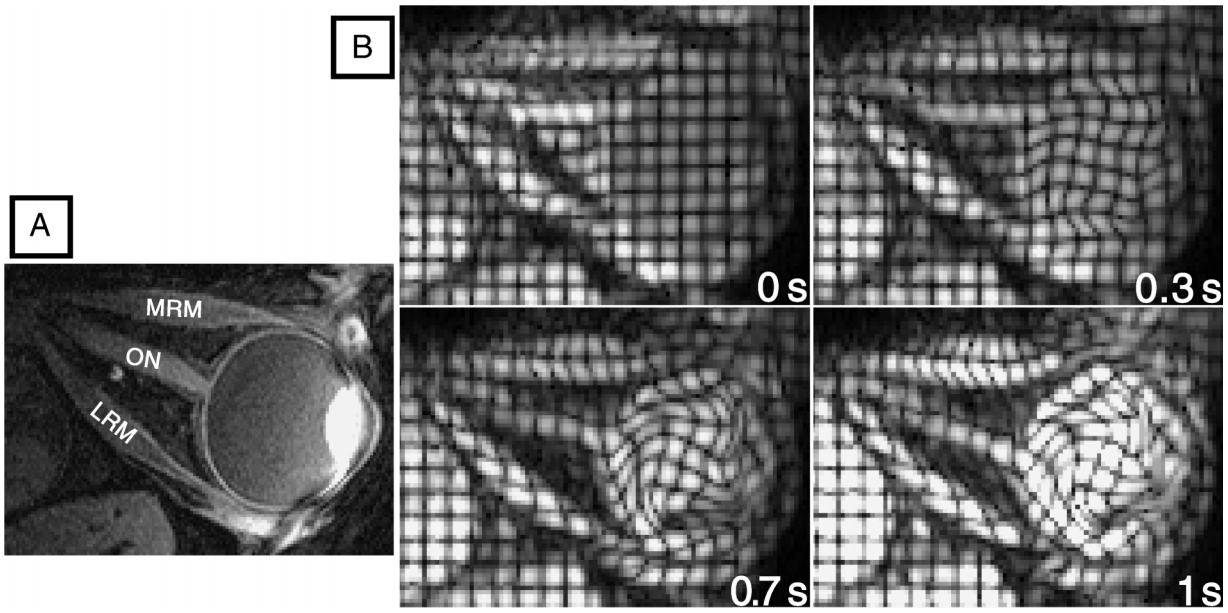

Figure 1. (A) Static MR image of the right orbit without tagging. The optic nerve (ON), the lateral rectus muscle (LRM), and the medial rectus muscle (MRM) are depicted in the image plane. (B) Four CSPAMM MR images of the same slice during eye movement. The magnetization is modulated to create a grid bind with the tissue (see time 0 s). The deformation of this grid (during time) depicts the differential movements within homogeneous tissues, such as in the extraocular muscles. The 1st, 5th, 10th, and 15th time frames are shown. The temporal resolution was 70 ms. These images are from the same subject (Subject 1).

are acquired, the magnetization of the tissue is periodically modulated in two perpendicular directions, so called tissue tagging. The resulting images look like anatomical images modulated by a grid pattern (see Figure 1B at time 0 s). The period of the sinusoidal modulation is termed the *tagline distance*. Since the modulation is used as marker, equivalent tissue markers are present at every tagline distance. As the magnetization moves with the underlying tissue, the displacement of each tissue point can be followed during the entire recording. The change of the distance between each marker was measured.

The postprocessing software assigns the nearest equivalent tissue point of the next time frame to each tissue point. As the postprocessing software cannot differentiate equivalent markers, the tagline distance should measure at least twice the maximal tissue displacement between two time frames. Otherwise, a movement in the wrong direction could be assigned to a tissue point. To select the appropriate tagline distance, the expected movement of the orbital tissue was calculated as follows: assuming the ocular globe including the adjacent connective tissues builds a 25- to 35-mm diameter sphere that rotates 64 deg/s during 70 ms (=4.5 deg) following the moving stimulus, the surface of such a sphere shifts 1.4 mm at most (4.5 deg*diameter*pi/360 deg). A tagline distance of at least a double sphere shift (3 mm) was needed. A larger tagline distance would increase the sensitivity of the measurement to noise and would consequently need extended scan time for compensation.

Postprocessing

An adapted software program based on TagTrack 1.5.6 (GyroTools Ltd.; Zurich; Switzerland) was used to track the marked tissue points automatically. The postprocessing

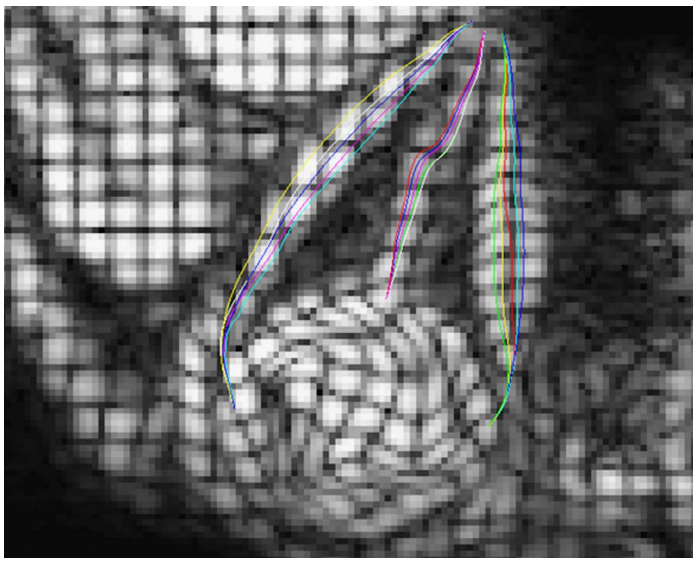

Figure 2. CSPAMM images of all 15 time frames including the manually embedded polylines (in color) in one subject (Subject 1) gazing from 20 deg right to 20 deg left. Five polylines served to track the two horizontal muscles and the optic nerve of the right eye.

method HARP (HARmonic Phase) (Osman, Kerwin, McVeigh, & Prince, 1999) with peak-combination (Ryf, Tsao, Schwitter, Stuessi, & Boesiger, 2004) is integrated into this software. HARP enables tracking of all tissue points, not just the tagging lines (dark lines of the grid), because it tracks the phase and not the MRI magnitude information. To understand motion-encoded MRI with HARP evaluation, it is important to distinguish the distance between equivalent markers (the tagline distance) from the acquired pixel size, which is always smaller. A circular band-pass filter was applied to extract the harmonic peaks in Fourier space and to diminish image noise. A filter diameter that doubles the image pixel size is the theoretical optimum of the HARP method. The size of the filter (which corresponds to a diameter of 2.7 pixels of the image) was selected as a trade-off between tracking stability and movement resolution. The filter was centered on the harmonic peak (of the sinusoidally modulated image) and enabled us to resolve a maximal contraction of 53% of the original tissue length at the first time frame. The maximal resolvable contraction with the optimal theoretic filter is given by the scan resolution (1.2 mm) divided by the tagging line distance (3 mm) (Osman et al., 1999), i.e., 40% (i.e., 2.5 times shorter). Hence, the degradation due to filtering is reasonable. There is no limitation for the maximal trackable elongation of a tissue.

The horizontal extraocular muscle thickness of about 3 mm (Kaufmann & Decker, 1995) was covered with at least one pixel that lay completely inside the muscle after filtering. Therefore, landmark chains traced and tracked on these pixels along the muscles were expected to describe similar motion. A good tracking technique should render similar motion for landmarks in the same pixel. To test the quality of the tracking algorithm, five landmark chains (=polylines) for each horizontal rectus muscle and the ON were manually drawn on the 10th time frame (approximately gaze straight ahead) such that the whole tissue broadness could be used for tracking (see Figure 2). For each polyline, TagTrack interpolated about 70 equally spaced points, and all of them were tracked through the 15 time frames. The standard deviation of the motion pattern of the polylines was calculated for the validation of the tracking algorithm. A small standard deviation corresponds to a good tracking quality of the algorithm. To ascertain that the polylines lay on the expected tissue, we took advantage of anatomical images and realigned the polylines if they were not on the muscles of interest. Although the signal to noise ratio dropped at the orbital apex, the tracking of the polylines was still reliable. The whole postprocessing procedure took in average 20 min for each subject.

Numerical and statistical evaluation of the polylines

The length of each polyline was defined as the sum of the distances between neighboring landmarks along the polyline. As reference length, the average of the length of the first and second time frames (20 deg right gaze) was selected. This improved the signal to noise ratio and was justified by the fact that the eye moved less than half a pixel during the first two time frames. The deformation (relative length change) of each polyline was calculated by dividing its length at the actual time frame by its reference length. Furthermore, each polyline was divided into three segments of equal length.

The changes of length of the horizontal rectus muscles as well as of the three EOM segments of the seven subjects were statistically analyzed by the Kruskal–Wallis test (ANOVA without Gaussian distribution assumption).

Results

Panels A and B of Figure 3 show representative tracking results of the right lateral rectus muscle (LRM), medial rectus muscle (MRM), and optic nerve (ON) of two different subjects. The LRMs of the right eye elongated +22% in Subject 1 and +19% in Subject 2 during 20 deg right to 20 deg left gaze. All five polylines of the LRM showed a consistent elongation as their standard deviations did not exceed 1% during the 15 time frames. Meanwhile, the MRMs of both subjects contracted from baseline to 83% with a length variation between the polylines of less than 2% in Subject 1 and 0.5% in Subject 2. The four times larger standard deviation of the MRM polylines of Subject 1 compared to Subject 2 is explained by the tracking imperfection of the polylines of the MRM of Subject 1: Polyline crossing can be observed on Figure 2 at the first time frame. As expected, the deformation patterns of both muscles were nearly sinusoidal corresponding to the sinusoidally oscillating right eye. The average length of the five polylines of the ON varied between 102% and 98% in Subject 1 and between 100% and 96% in Subject 2. For Subject 2, the standard deviation of the five polylines of the ON was slightly greater than in the two rectus muscles but was still smaller than 2%. Subject 1 did not show a greater standard deviation of the ON polylines compared to the EOM polylines. The mean of the standard deviation of all subjects at each single time frame was smaller than 1% for the three tissues.

The actual lengths of the polylines of the three tissues at the first and last time frames are listed in Panels 3C and 3D. To unambiguously compare the lengths of the different polylines, we consider in this paragraph the average of the lengths at the first and last time frames. For Subject 1, the LRM was slightly longer than the MRM, and the ON was the shortest, as expected. However, the length analysis of the polylines of Subject 2 revealed that the polylines did not represent the whole length of the labeled tissue, as the LRM polylines were shorter than the MRM polylines. The anterior part of

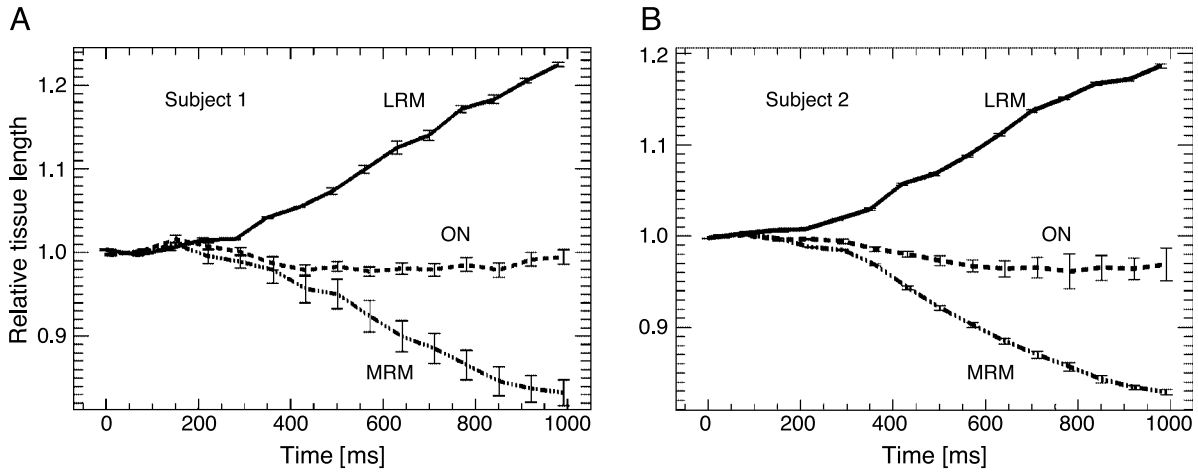

C

Tissue lengths of Subject 1 [mm]

	20° Right gaze	20° Left gaze
LRM	36.1 ± 0.6	44.1 ± 0.7
ON	26.0 ± 0.4	26.0 ± 0.1
MRM	39.7 ± 0.8	33.1 ± 0.1

D

Tissue lengths of Subject 2 [mm]

	20° Right gaze	20° Left gaze
LRM	29.8 ± 0.2	35.4 ± 0.2
ON	23.5 ± 0.2	22.5 ± 0.5
MRM	40.5 ± 0.1	33.6 ± 0.2

Figure 3. (A, B) Change of length relative to the tissue length at the first time frame at 20 deg right gaze. The five polylines of the relaxing lateral rectus muscle (LRM), the optic nerve (ON), and the contracting medial rectus muscle (MRM) of the right eye are averaged. The tissue deformations of two subjects are depicted during 1 s (from 20 deg right to 20 deg left gaze). The movements of the muscles and the optic nerve were distinguishable from each other (error bars: ±one standard deviation). (C, D) Length of the polylines of each tissue (of Subjects 1 and 2) averaged for the five polylines at the first and last time frame (errors: ±one standard deviation).

the LRM of Subject 2 was relatively thin so that it was not possible to get reliable tracking of this muscle region.

Both horizontal EOMs and the ON of Subject 2 were further investigated in more details. The top Panel of Figure 4 shows the LRM of this subject. This muscle was divided into three segments of equal lengths (at straight-ahead gaze). The middle segment of the muscle (muscle belly) elongated twice as much as the anterior and the posterior segments. This result is expected, since the anterior and the posterior segments of the muscles contain more tendon that cannot stretch as easily as muscle tissue. The larger standard deviation of the five polylines at the 15th time frame in the middle and posterior part of the LRM segments was due to partial volume effects that appeared at the interface of tissues with different movements. These effects occurred also in the anterior part of the EOM in other subjects.

Relative to the posterior and anterior part of the muscle, the middle segment of the LRM relaxed earlier and to a larger extent in later time frames. In contrast to the heterogeneously contracting LRM segments, the three ON segments all had a similar degree of longitudinal deformation (Figure 4—central Panel). In this subject, the standard deviations among the five polylines of the ON segments were greater than in the LRM; however, this was not the case for all subjects.

The bottom Panel of Figure 4 shows the heterogeneous contraction among the three medial rectus segments. The middle segment contracted ahead of the anterior and posterior segments. This pattern of earlier contraction extended even to the later time frames. The standard deviation of the five polylines in each segment was comparable to the segments of the LRM (Figure 4—top Panel). In fact, the average of all subjects' standard deviation at each single time frame was smaller than 3% for each segment of the three tissues.

The Figures 5 and 6 summarize the results in all seven subjects. Figure 5 shows a clear separation among the LRM elongation, the ON deformation, and the MRM contraction. The standard deviation among the subjects increased over time and was slightly more pronounced in the LRM and the ON than in the MRM. This may be due to the nonlinearity of the deformation scale. Since the standard deviation of the subjects was relatively small, there was a statistically significant separation of the two horizontal EOMs after the third time frame (corresponding to a gaze deviation of 1.9 deg from the 20 deg right gaze; see * at 140 ms), and of the three tissues from each other after the fourth time frame (corresponding to a gaze deviation of 4.2 deg from the 20 deg right gaze; see ** at 210 ms).

Figure 6 depicts the heterogeneous longitudinal segmental deformation of the LRM (top Panel), the ON

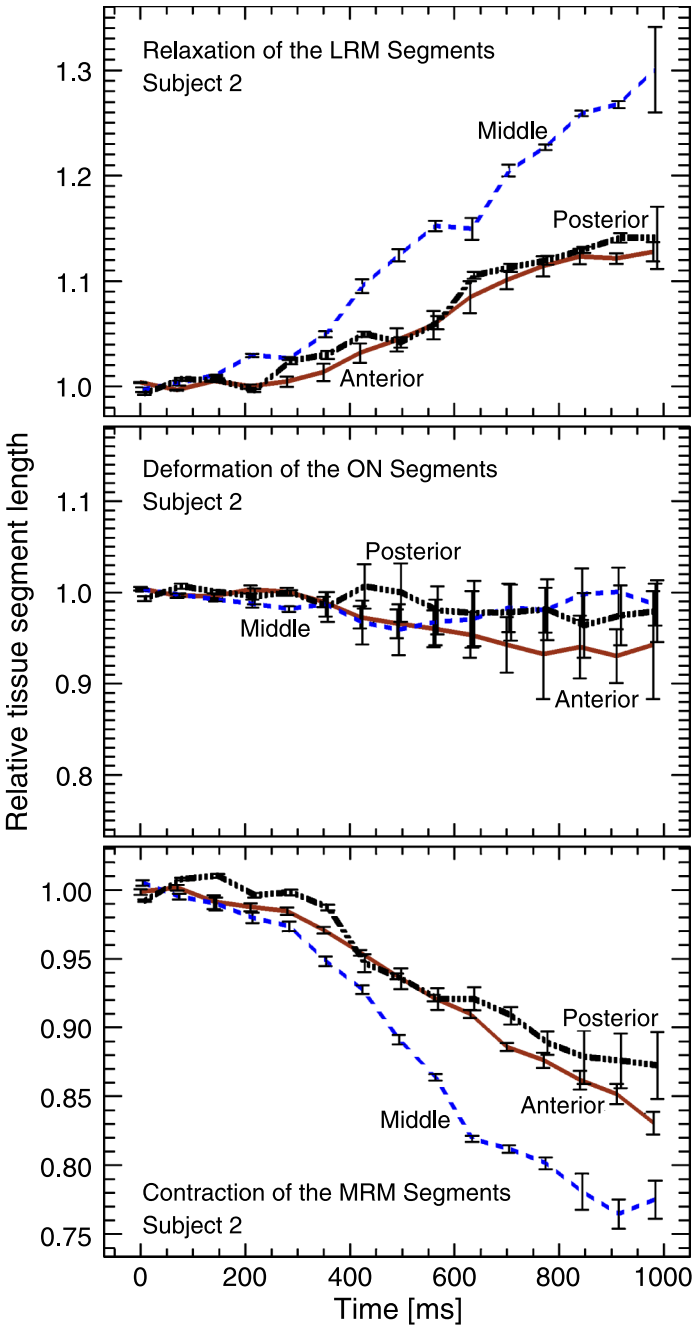

Figure 4. Change of relative tissue length of Subject 2 averaged for the five polylines. The lateral rectus muscle (LRM, top Panel), the optic nerve (ON, central Panel), and the contracting medial rectus muscle (MRM, bottom Panel) are divided into three segments. The lengths of the segment closest to the eye globe (anterior, brown), the muscle belly or the optic nerve mid portion (middle, blue), and the orbital apex segment (posterior, black) are analyzed. In both horizontal rectus muscles, the middle segments can be distinguished from the anterior and posterior segments. In the optic nerve, however, all segments were similarly distorted (error bars: ±one standard deviation).

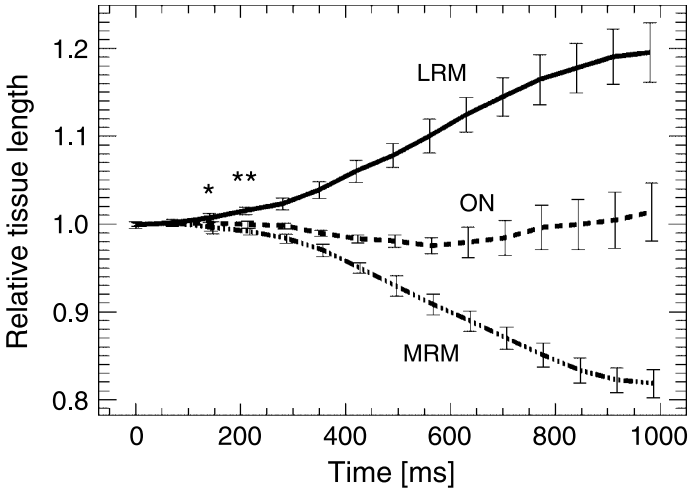

Figure 5. Change of length relative to the length at the first time frame for the relaxing lateral rectus muscle (LRM), the optic nerve (ON), and the contracting medial rectus muscle (MRM) during 1 s of eye movement, averaged over the seven subjects. The standard deviation among the subjects was small. A single asterisk (*) indicates that the LRM and MRM were statistically significantly distinguished from the third time frame on corresponding to a gaze deviation of 1.9 deg. Two asterisks (**) indicate that all three tissues were statistically significantly distinguished from the fourth time frame on corresponding to a gaze deviation of less than 4.2 deg (error bars: ±one standard deviation).

(central Panel), and the MRM (bottom Panel). All length changes were expressed relative to the averaged length of the first two time frames and averaged for all seven subjects. The greatest relaxation of the LRM was present in the middle segment of the muscle and was greater in the orbital apex than in the anterior segment. The difference between the relaxation of the different muscle segments was statistically significant, so that the muscle segments could be distinguished after just a brief period of eye movement. Examining the LRM (Figure 6—top Panel), the anterior segment was statistically significantly distinguishable from the other two segments from the fourth time frame on (210 ms, see *). From the ninth time frame on (560 ms, see **), all three segments were statistically significantly distinguishable from each other. The separation among the ON segments was not statistically significant in all time frames (Figure 6—central Panel). Considering the MRM (Figure 6—bottom Panel), the middle segment was statistically significantly stronger contracting than the other two segments from the sixth time frame on (350 ms, see *). From the seventh time frame on (420 ms, see **), all three segments were statistically significantly distinguishable from each other.

In summary, the posterior and the middle segments of the LRM were the earliest to relax, whereas the middle segment was the earliest to contract in the MRM.

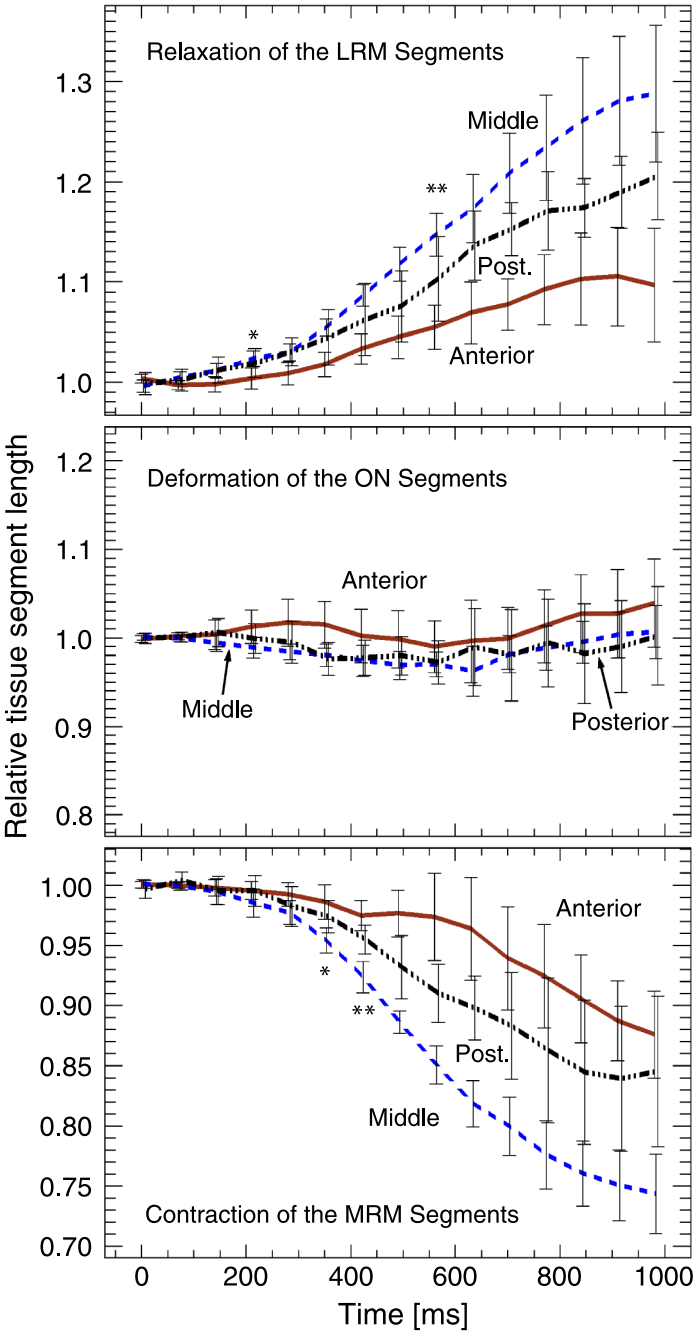

Figure 6. Change of relative tissue length averaged for the seven subjects. The lateral rectus muscle (LRM, top Panel), the optic nerve (ON, central Panel), and the contracting medial rectus muscle (MRM, bottom Panel) are divided into three segments. The segment closest to the eye globe (anterior, brown), the muscle belly or the optic nerve mid portion (middle, blue), and the orbital apex segment (posterior, black) are depicted. The three segments can be distinguished from each other for both muscles, but are similar for the ON (error bars: ±one standard deviation). A single asterisk (*) indicates that, from that time frame on, one segment was statistically significantly distinguishable from the other two. Two asterisks (**) indicate that all three segments were statistically significantly distinguishable from each other.

Discussion

Main findings

Motion-encoded MRI can be successfully used to analyze patterns of EOM contraction during smooth pursuit eye movement. Because the variability among healthy subjects was small, statistically significant differences among the anterior, middle, and posterior segments of the EOMs could be identified. Greater deformation of the muscles was seen nearer to the orbital apex than to the anterior segment of the muscle. As a control, the deformation along the ON was homogeneous.

In both horizontal EOMs, the anterior segment was the last segment that deformed. This may be due to the great percentage of tendon within this segment. Nevertheless, there was a slightly different distribution of the pattern of deformation between the lateral and medial rectus muscles. The posterior segment of the LRM relaxed before the comparable segment in the MRM contracted. One can speculate about the heterogeneous pattern of deformation between the two muscles. The dynamics of the deformation pattern of a muscle could be different during contraction and relaxation. Future experiments, including the analysis of the eye movement in the other (left-to-right) horizontal direction, may find such a difference.

Image acquisitions and postprocessing of motion-encoded MRI

One advantage of the motion encoding technique in comparison to conventional MRI is that tissue deformation can be resolved. Since the magnetic property of the orbital tissues is modulated, it can be used as marker for the tissue deformation. Moreover, this method is non-invasive, i.e., no physical markers are necessary to track the deformation of orbital tissue while the eye is moving. Since motion-encoded MRI resolves motion and hence does not need to resolve tissue borders, supramillimetric resolution imaging was sufficient for separating the motion of the three EOM segments during smooth pursuit eye movement. The signal to noise ratio can be improved by employing a small coil, as has been used for tracking blood flow (Morse & Singer, 1970) and for orbital imaging (Schenck et al., 1985). In addition, the relatively small sensitivity zone of a small coil allows using a small field of view that further shortens image acquisition time. The signal to noise ratio drop with depth (due to the small diameter of the coil) was more than compensated by its greater sensitivity.

The standard deviations of the tissue deformation were small in each subject, demonstrating the reproducibility of the automatic tracking of the polylines. The five polylines in each muscle did not constitute independent measures.

The reproducibility of the tissue point tracking worsened in the time frames at the end of the tracking. Due to the drop of signal to noise ratio with a greater number of time frames, the acquisition was limited only to the right-to-left gaze phase of the horizontal sinusoidal movement. A possible solution to enhance the tracking quality would be to track the five polylines as a whole and not as separated entities. This should reduce the noise sensitivity of the tracking and may also reduce the acquisition time or allow a greater number of segments along the muscles to be resolved. In this context, it is noteworthy that a good shimming (homogenization of the static magnetic field) prior to image acquisition is essential when using the described technique. The gradient echo EPI sequence used for faster acquisition in this study is sensitive to the magnetic susceptibility artifacts (Chen, Chandna, & Abernethy, 2005), which are prominently present in the orbit (Herrick, Hayman, Taber, DiazMarchan, & Kuo, 1997).

The polyline tracking software TagTrack works with hand drawn polylines on the motion-encoded image. To ascertain that the polylines lay on the expected tissue, we took advantage of anatomical images and realigned the polylines if they were not on the muscles of interest or the ON. Drawing polylines on the anatomical image, and a subsequent automatic transfer to the motion-encoded image, would improve the position accuracy of the polylines.

Motion-encoded MRI acquires images during several time frames (see Figure 1) during a single acquisition. To maintain a reasonable scan time, the scan resolution was ten times lower than the one used for high-resolution conventional MRI (Kau, Tsai, Ortube, & Demer, 2007). An evident limitation of the low resolution is the inability to resolve diverse structures within EOMs, as, for example, the global and orbital EOM layers. Nevertheless, as about twenty pixels are acquired in the longitudinal direction of the muscles, this method was capable of resolving three muscle segments. The limited resolution mainly affects the interface of differently moving tissues. Since the anterior segments of the EOMs are thin, their tracking was more difficult than the middle or posterior segments (Figure 3). To diminish the partial volume effect in the outer layer of the EOMs, the signal was optimized by taking advantage of the specific T1 of muscles. Note that the tagline distance is not important for resolution. The tagline distance gives only the period of the phase information. The resolution of the phase information used for the tracking is limited by the scan resolution and the size of the postprocessing filter.

Detection of motion of extraocular muscles

Several prior studies attempted to resolve the deformation of the orbital tissues induced by different eye positions. CT (Simonsz, Harting, De waal, & Verbeeten, 1985) and MRI studies segmented static coronal images to determine the contraction pattern of the extraocular recti muscles (Miller, 1989) and the two oblique muscles (Kono & Demer, 2003) by measuring the cross-sectional area of the muscles. Coronal images represent a fixed section of space through which the EOMs are shown at a specific eye position. One should be aware that motion of EOMs through the fixed planes of images can result in apparent motion and thickening of a region simply due to the geometric effect of tangentially cutting through the curved surfaces of the EOMs as they are pulled through the imaging plane. Although pull-through effects may change the apparent thickness of the EOMs, they will not change the spacing of the tagging lines as used in the present study, permitting pull-through effects to be distinguished from true contraction.

Another attempt to depict movement in the orbit was to image eye positions in transversal planes (Abràmoff, Van Gils, Jansen, & Mourits, 2000; Botha et al., 2005). Such a method is valid for following tissue borders and not for describing contractility within tissues, since heterogeneous deformation inside homogeneously contrasted tissues cannot be assigned with certainty due to the absence of landmarks for deformation recognition. Recognizing the necessity of such landmarks, Miller et al. (2006) implanted gold beads inside monkey orbits, that served to successfully demonstrate orbital soft tissue deformation in static CT acquisitions.

All these methods used static images. However, the nomenclature is not standardized. Shin, Demer, and Rosenbaum (1996) stated that "dynamic imaging refers to viewing the EOMs during different maintained gaze positions." Abràmoff et al. (2000) and Bailey et al. (1993) named the same imaging method "cine imaging." Recently, Kau et al. (2007) designated it as "multi positional imaging," which seems most appropriate to describe multiple static imaging, as it is not associated with motion. On the other hand, "motion-encoded MRI" refers to imaging using a motion encoding feature and multiple time frames acquired during eye movement. In this paper, we restricted the analysis to the change of muscle length. The muscle path and contraction patterns may differ during the actual eye movement in comparison to the static condition, as the force and torque resultants do not need to be null during the eye movement (Weber, Bockisch, Bergamin, Landau, & Straumann, 2005).

In the future, we plan to upgrade the tracking algorithm of the polylines in order to sample the EOMs in more than three segments. To further enhance the spatial resolution of the images, a specialized coil array will be needed. Our method has the potential of improving the temporal resolution without the need to adapt other scan parameters. With a better temporal resolution, EOMs contraction may be imaged during saccades. To reach this goal, the accuracy of the eye movement needs to be verified with simultaneous eye movement measurements.

Conclusion

Motion-encoded MRI of the orbit during eye movement is a versatile and noninvasive method which permits detailed studies of normal and pathologic EOMs in vivo with good resolution of the deformation of soft orbital tissues, even in regions where physical markers or devices cannot easily be implanted, such as the orbital apex. This methodology may have a number of potential clinical benefits by identifying specific patterns of deformation in different diseases of the orbital muscles (e.g., thyroid orbitopathy, orbital pseudotumor) or in conditions which alter the innervation to eye muscles (e.g., acquired or congenital aberrant innervation).

Acknowledgments

We thank the Swiss National Science Foundation (SNF #3100AO-102197) for grant support. This work was rewarded by the Gesine Mohn Travel Grant Award (ARVO 2006).

Commercial relationships: none.
Corresponding author: Oliver Bergamin.
Email: Oliver.Bergamin-remy@usz.ch.
Address: Department of Ophthalmology, University Hospital of Zurich, Frauenklinikstrasse 24, CH-8091 Zurich, Switzerland.

References

Abràmoff, M. D., Van Gils, A. P., Jansen, G. H., & Mourits, M. P. (2000). MRI dynamic color mapping: A new quantitative technique for imaging soft tissue motion in the orbit. *Investigative Ophthalmology & Visual Science, 41,* 3256–3260. [PubMed] [Article]

Axel, L., & Dougherty, L. (1989). MR imaging of motion with spatial modulation of magnetization. *Radiology, 171*, 841–845. [PubMed] [Article]

Bailey, C. C., Kabala, J., Laitt, R., Weston, M., Goddard, P., Hoh, H. B., et al. (1993). Cine magnetic resonance imaging of eye movements. *Eye, 7,* 691–693. [PubMed]

Botha, C., de Graaf, T., Root, R., Wielopolski, P., Schutte, S., Post, F., et al. (2005). Time-varying three-dimensional vector field visualisation for the analysis of retrobulbar fat mobility during eye motion. *Proceedings of the 11th Annual Conference of the Advanced School for Computing and Imaging* (pp. 1–5).

Chen, S. I., Chandna, A., & Abernethy, L. J. (2005). Magnetic susceptibility artifact in orbital magnetic resonance imaging. *Strabismus, 13,* 1–3. [PubMed] [Article]

Fischer, S. E., Mckinnon, G. C., Maier, S. E., & Boesiger, P. (1993). Improved myocardial tagging contrast. *Magnetic Resonance in Medicine, 30,* 191–200. [PubMed]

Herrick, R. C., Hayman, L. A., Taber, K. H., Diaz-Marchan, P. J., & Kuo, M. D. (1997). Artifacts and pitfalls in MR imaging of the orbit: A clinical review. *Radiographics, 17,* 707–724. [PubMed] [Article]

Kau, H. C., Tsai, C. C., Ortube, M. C., & Demer, J. L. (2007). High-resolution magnetic resonance imaging of the extraocular muscles and nerves demonstrates various etiologies of third nerve palsy. *American Journal of Ophthalmology, 143,* 280–287. [PubMed]

Kaufmann, H., & Decker, W. d. (1995). Strabismus (2nd ed., p. 37). Stuttgart: Enke.

Kono, R., & Demer, J. L. (2003). Magnetic resonance imaging of the functional anatomy of the inferior oblique muscle in superior oblique palsy. *Ophthalmology, 110,* 1219–1229. [PubMed]

Meyer, C. H., Lasker, A. G., & Robinson, D. A. (1985). The upper limit of human smooth pursuit velocity. *Vision Research, 25,* 561–563. [PubMed]

Miller, J. M. (1989). Functional anatomy of normal human rectus muscles. *Vision Research, 29,* 223–240. [PubMed]

Miller, J. M., Rossi, E. A., Wiesmair, M., Alexander, D. E., & Gallo, O. (2006). Stability of gold bead tissue markers. *Journal of Vision, 6*(5):6, 616–624, http://journalofvision.org/6/5/6/, doi:10.1167/6.5.6. [PubMed] [Article]

Morse, O. C., & Singer, J. R. (1970). Blood velocity measurements in intact subjects. *Science, 170,* 440–441. [PubMed]

Osman, N. F., Kerwin, W. S., McVeigh, E. R., & Prince, J. L. (1999). Cardiac motion tracking using CINE harmonic phase (HARP) magnetic resonance imaging. *Magnetic Resonance in Medicine, 42*, 1048–1060. [PubMed]

Ryf, S., Tsao, J., Schwitter, J., Stuessi, A., & Boesiger, P. (2004). Peak-combination HARP: A method to correct for phase errors in HARP. *Journal of Magnetic Resonance Imaging, 20,* 874–880. [PubMed]

Schenck, J. F., Hart, H. R., Jr., Foster, T. H., Edelstein, W. A., Bottomley, P. A., Redington, R. W., et al. (1985). Improved MR imaging of the orbit at 1.5 T with

surface coils. *American Journal of Roentgenology, 144,* 1033–1036. [PubMed] [Article]

Shin, G. S., Demer, J. L., & Rosenbaum, A. L. (1996). High resolution, dynamic, magnetic resonance imaging in complicated strabismus. *Journal of Pediatric Ophthalmology and Strabismus, 33,* 282–290. [PubMed]

Simonsz, H. J., Harting, F., de Waal, B. J., & Verbeeten, B. W. (1985). Sideways displacement and curved path of recti eye muscles. *Archives of Ophthalmology, 103,* 124–128. [PubMed]

Soellinger, M., Ryf, S., Boesiger, P., & Kozerke, S. (2007). Assessment of human brain motion using CSPAMM. *Journal of Magnetic Resonance Imaging, 25,* 709–714. [PubMed]

Suryan, G. (1951). Nuclear resonance in flowing liquids. *Proceedings of the Indian Academy of Science A, 33,* 107–111.

Weber, K. P., Bockisch, C. J., Bergamin, O., Landau, K., & Straumann, D. (2005). Modulation of saccade curvature during Bielsehowsky head-tilt testing in patients with unilateral trochlear nerve palsy and healthy subjects. *Journal of the Neurological Sciences, 238,* S48.

Yee, R. D., Goldberg, R. A., Jones, O. W., Baloh, R. W., & Honrubia, V. (1983). Effect of eccentric gaze on pursuit. *Investigative Ophthalmology & Visual Science, 24,* 1108–1114. [PubMed] [Article]

Zerhouni, E. A., Parish, D. M., Rogers, W. J., Yang, A., & Shapiro, E. P. (1988). Human heart: Tagging with MR imaging—A method for noninvasive assessment of myocardial motion. *Radiology, 169,* 59–63. [PubMed] [Article]